Spectroscopic Studies of Side-On Peroxide-Bridged Binuclear Copper(II) Model Complexes of Relevance to Oxyhemocyanin and Oxytyrosinase

Michael J. Baldwin,[†] David E. Root,[†] James E. Pate,[‡] Kiyoshi Fujisawa,[§] Nobumasa Kitajima,[§] and Edward I. Solomon*,[†]

Contribution from the Department of Chemistry, Stanford University, Stanford, California 94305, Research Laboratory of Resource Utilization, Tokyo Institute of Technology, 4259 Nagatsuta, Midori-ku, Yokohama 227, Japan, and Advanced Polymeric Systems Laboratory, Dow Chemical Company, Central Research, Midland, Michigan 48674. *Received May 28, 1992*

Abstract: Spectrosopic studies on two side-on μ-η^2:η^2 peroxide-bridged cupric dimers, $[Cu(HB(3,5\text{-}R_2pz)_3)]_2(O_2)$, where $(HB(3,5\text{-}R_2pz)_3)$ is a tris(pyrazolyl)borate ligand and R = *i*-Pr or Ph, are presented and compared to our previous studies of end-on bound(η^1) peroxide-coppper monomer and bridged dimer (trans-μ-1,2) complexes. Two transitions at 350 nm (ϵ = 26000 M^{-1} cm^{-1}) and 538 nm (ϵ = 2000 M^{-1} cm^{-1}) are assigned as peroxide-to-copper charge-transfer transitions. A method has been developed to quantitate electron density donation from the ligand to the metal center using the intensity of the ligand-to-metal charge-transfer transitions. It is found that the side-on bridging peroxide donates significantly more electron density from the peroxide π^* orbitals to the coppers than does peroxide in end-on bound monomer and dimer complexes. The amount of charge donation is proportional to the number of σ bonds between the peroxide and the coppers (side-on bridged dimer = 4, end-on bridged dimer = 2, end-on monomer = 1). The increased charge donation results in a less negative peroxide in the side-on complex and should in principle produce a stronger O–O bond. Four vibrational modes are assigned in the resonance Raman and infrared spectra on the basis of isotopic shifts at 763 (rR, 723 cm^{-1} with $^{18}O_2$), 331 (IR, 321 cm^{-1} with $^{18}O_2$), 284 (rR, no shift with $^{18}O_2$), and 572 cm^{-1} (based on an overtone at 1144 cm^{-1} in rR, 1098 cm^{-1} with $^{18}O_2$) in the R = Ph complex, with corresponding peaks at 749, 285, and 1055 cm^{-1} in the resonance Raman spectra of the R = *i*-Pr complex. A normal coordinate analysis shows that the oxygen–oxygen force constant, $k_{O\text{-}O}$, is smaller in the side-on bridged complex (2.4 mdyn/Å) than in the end-on monomer (2.9 mdyn/Å) or end-on bridged dimer (3.1 mdyn/Å), and thus the O–O bond is weaker in the side-on complex than in the end-on, despite its greater peroxide charge donation. This is direct evidence for the π acceptor ability of the peroxide in this side-on bridged structure, which involves some peroxide σ^* character mixing into the highest energy occupied molecular orbital, as predicted by Xα calculations [Ross, P. K.; Solomon, E. I. *J. Am. Chem. Soc.* **1991**, *113*, 3246-3259]. Using the correlation of charge-transfer intensities to ligand charge donation, the charge-transfer intensity of oxyhemocyanin indicates that it likely has four copper–peroxide bonds and thus a side-on peroxide bridging structure. The electronic structure of this side-on bridging geometry in oxyhemocyanin explains its unique spectroscopic features, including the high intensity and energy of the 345-nm absorption band, the low O–O stretching frequency, and the lack of a symmetric Cu–O stretch in the expected energy range of the resonance Raman spectrum. This electronic structure also provides insight into the mechanisms of oxygen binding and activation in hemocyanin and tyrosine.

I. Introduction

Oxyhemocyanin, the oxygen transport protein in arthropods and molluscs, has a binuclear copper(II) active site which is bridged symmetrically by peroxide.[1,2] The monooxygenase tyrosinase, which activates oxygen for the oxygenation of phenols to *o*-diphenols, has been shown to have an active site similar to that of oxyhemocyanin.[3] Each has intense peroxide-to-copper charge-transfer (CT) transitions, with absorption bands at 350 (ϵ =20000 M^{-1} cm^{-1}) and 570 nm (ϵ = 1000 M^{-1} cm^{-1}) and a circular dichroism (CD) band at 480 nm with little corresponding absorption intensity.[1] In a copper–peroxide monomer[4] complex (Figure 1A), two peroxide-to-copper CT transitions are expected, one from each of the pair of π^* orbitals, which are the highest energy occupied molecular orbitals (HOMOs) of peroxide. One of these π^* orbitals undergoes a σ-bonding interaction with the half-occupied copper d orbital and is designated as π^*_σ. This bonding interaction stabilizes this π^* orbital relative to the other, which is designated as π^*_ν. Thus, the $\pi^*_\sigma \rightarrow$ Cu CT transition is higher in energy and more intense (due to greater overlap with the half-occupied copper $d_{x^2-y^2}$ HOMO) than the $\pi^*_\nu \rightarrow$ Cu CT transition. Since there are more than two peroxide-to-copper CT transitions observed in oxyhemocyanin, the peroxide must bridge the two coppers.[1] The 350-nm absorption band has been assigned as the $\pi^*_\sigma \rightarrow$ Cu CT transition and the 570-nm absorption and 480-nm CD band as two components of the $\pi^*_\nu \rightarrow$ Cu CT transition. The two components derive from the fact that the peroxide bridges the two coppers, so that each monomer transition splits into symmetric and antisymmetric combinations in the dimer. On the basis of spectroscopic and chemical studies on oxyhemocyanin, including a transition vector dipole coupling analysis[1] of these optical spectra and EXAFS studies,[5] which indicate a 3.6 Å Cu–Cu distance, a cis-μ-1,2 peroxide bridging mode (Figure 1B) was proposed as being the only geometry known at that time for any transition metal–peroxide complex which was consistent with the spectroscopic data. This is a common structure for peroxide-bridged cobalt dimers;[6] however, no copper–peroxide complexes had yet been prepared when this structure was proposed. Karlin later prepared[7] copper complexes with peroxide bound end-on to one copper[8] (Figure 1A) and peroxide bridging two coppers in a trans-μ-1,2 manner[9] (Figure 1C); the latter was structurally characterized by X-ray crystallography.[10] We have

[†] Stanford University.
[‡] Dow Chemical Company.
[§] Tokyo Institute of Technology.

(1) Eickman, N. C.; Himmelwright, R. S.; Solomon, E. I. *Proc. Natl. Acad. Sci. U.S.A.* **1979**, *76*, 2094-2098.
(2) Thamann, T. J.; Loehr, J. S.; Loehr, T. M. *J. Am. Chem. Soc.* **1977**, *99*, 4187-4189.
(3) Himmelwright, R. S.; Eickman, N. C.; LuBien, C. D.; Lerch, K.; Solomon, E. I. *J. Am. Chem. Soc.* **1980**, *102*, 7339-7344.
(4) In this paper, the term "monomer" refers to peroxide bound to a single copper ion; the term "dimer" refers to a peroxide bridging a pair of copper ions and mediating interactions between these copper ions.
(5) Co, M. S.; Hodgson, K. O.; Eccles, T. K.; Lontie, R. *J. Am. Chem. Soc.* **1981**, *103*, 984-986.
(6) Barraclough, C. G.; Lawrence, G. A.; Lay, P. A. *Inorg. Chem.* **1978**, *17*, 3317-3322.
(7) Karlin, K. D.; Cruse, R. W.; Gultneh, Y.; Farooq, A.; Hayes, J. C.; Zubieta, J. *J. Am. Chem. Soc.* **1987**, *109*, 2668-2679.
(8) (a) This complex, $[Cu_2(XYL\text{–}O\text{–})(O_2)]^+$, contains two copper ions, but the peroxide has been shown by resonance Raman spectroscopy to bind to only one of the Cu(II)'s.[8b] (b) Pate, J. E.; Cruse, R. W.; Karlin, K. D.; Solomon, E. I. *J. Am. Chem. Soc.* **1987**, *109*, 2624-2630.
(9) Baldwin, M. J.; Ross, P. K.; Pate, J. E.; Tyeklár, Z.; Karlin, K. D.; Solomon, E. I. *J. Am. Chem. Soc.* **1991**, *113*, 8671-8679.

0002-7863/92/1514-10421$03.00/0

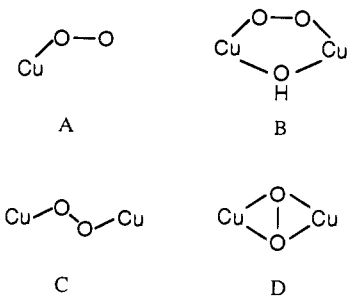

Figure 1. Peroxide–copper binding modes: (A) end-on monomer; (B) end-on cis-μ-1,2 dimer with a second OH^- bridge; (C) end-on trans-μ-1,2 dimer; (D) side-on μ-η^2:η^2 dimer.

Scheme I

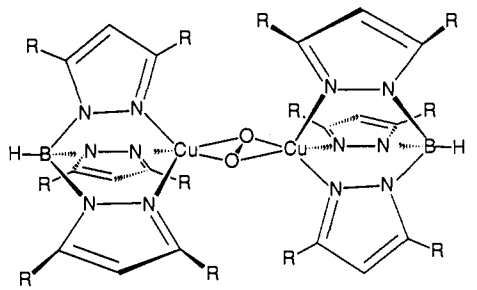

studied the absorption and resonance Raman features of these two complexes in detail in refs 8 and 9. Neither of these complexes had spectroscopic features consistent with oxyhemocyanin's intense peroxide-to-copper charge-transfer absorption band at 350 nm nor its unusually low frequency O–O stretch (750 cm^{-1})[11,12] in the resonance Raman spectrum. In addition, both exhibit a symmetric Cu–O_2 stretch in the 400–600 cm^{-1} region which is absent in this region of the resonance Raman spectrum of oxyhemocyanin.[11,12] In 1989, the X-ray crystal structure for the side-on peroxide-bridged copper dimer which is the subject of this paper was published by Kitajima and co-workers.[13] This complex (Scheme I) was the first structurally characterized example of the side-on bridging mode for peroxide in transition metal complexes and added an alternative structure (Figure 1D) to be considered for the active sites of oxyhemocyanin and oxytyrosinase.

Broken-symmetry self-consistent field–Xα–scattered wave (SCF-Xα-SW) calculations by Ross and Solomon[14] comparing the possible binding modes of peroxide to copper showed that the proposed cis-μ-1,2 model should have an electronic structure similar to that of the trans-μ-1,2 complex studied previously.[9] The calculations showed, however, that the side-on bridging model should have a significantly different electronic structure. Among the most interesting differences are the occupation of two coordination positions on each copper by peroxide for the side-on model compared to one for the end-on models, resulting in potentially stronger σ donation by peroxide π^* orbitals and the presence of peroxide σ^* character in the highest occupied molecular orbital (HOMO) in the side-on model, shifting some electron density into a highly antibonding orbital of peroxide. The solution spectral features of the side-on bridged complex[15] appear consistent with those of oxyhemocyanin, including the low O–O stretching frequency and the high-energy, intense peroxide-to-copper charge-transfer band; however, there has been some concern as to the origin of these spectroscopic features.[16,17] It has been suggested that a mixture of this complex and a superoxide complex[16] exists in solution to produce the various spectral features which appear consistent with oxyhemocyanin. We have therefore first addressed the question of which features correspond to the structurally characterized complex with a series of experiments comparing the solution data to the spectral features of the structurally defined microcrystalline solid.

This spectroscopic study of the μ-η^2:η^2 side-on peroxide-bridged copper dimers, $[Cu(HB(3,5\text{-}R_2pz)_3)]_2(O_2)$, where R = *i*-Pr or Ph and $(HB(3,5\text{-}R_2pz)_3)$ is a tris(pyrazolyl)borate ligand, extends a series of studies in our lab which began with the end-on bound monomer prepared by Karlin[8] compared to a trans-μ-1,2 end-on peroxide-bridged copper dimer[9] and now compares these end-on bound peroxide–copper complexes to the side-on bridged dimer. The experimentally derived electronic structures of these complexes are compared in light of the differences predicted by the Xα calculations,[14] showing important, newly defined properties of the side-on peroxide bridging mode. In addition, the unique normal mode structure of the side-on bridged complex is investigated by a normal coordinate analysis of the isotopically perturbed vibrations of the Cu_2O_2 core identified in the resonance Raman and infrared spectra. Finally, the integrated intensities of the peroxide-to-copper charge-transfer transitions for the series monomer → end-on dimer → side-on dimer are used to derive the amount of peroxide donation to the copper, which is shown to be proportional to the number of peroxide–copper σ-bonding interactions and relates to the relative charge on the peroxide in each of these complexes. On a quantitative level, the spectral features of oxyhemocyanin support a side-on peroxide-bridged structure for its active site. Our electronic studies of the μ-η^2:η^2 bridge define the origin of its unique spectral features and provide key insight into electronic contributions to oxygen binding and activation by hemocyanin and tyrosinase.

II. Experimental Section

The purple $[Cu(HB(3,5\text{-}i\text{-}Pr_2pz)_3)]_2(O_2)$ is prepared by reacting the blue bis-hydroxide-bridged Cu(II) precursor, $[Cu(HB(3,5\text{-}i\text{-}Pr_2pz)_3)]_2(\mu\text{-}OH)_2$, prepared as previously described,[15,17] with hydrogen peroxide in methylene chloride at −20 °C. The microcrystalline material is obtained by removing the solvent by vacuum until crystalline material stops forming on the walls of the flask, removing the remaining solution and discarding it, and drying the crystals further by vacuum. The purple $[Cu(HB(3,5\text{-}Ph_2pz)_3)]_2(O_2)$ was prepared by adding O_2 gas to a flask containing the yellow monomeric Cu(I) precursor, $Cu(Me_2CO)(HB(3,5\text{-}Ph_2pz)_3)$, prepared as previously described,[17] in a methylene chloride solution at −20 °C and precipitating the solid at −80 °C. The isotopically substituted complex was prepared using 98% $^{18}O_2$. Both of the peroxide complexes are thermally unstable and were stored at −80 °C, although the solid $[Cu(HB(3,5\text{-}Ph_2pz)_3)]_2(O_2)$ is reasonably stable at room temperature for time periods on the order of an hour.

The UV/vis spectra were taken on a Cary 17 spectrophotometer interfaced to a Compaq 386 personal computer with OLIS (on line instrument services) software. Samples were placed in an Oxford variable-temperature liquid nitrogen optical cryostat. The samples for the $[Cu(HB(3,5\text{-}i\text{-}Pr_2pz)_3)]_2(O_2)$ mull spectra were prepared in a glove bag filled with dry nitrogen gas by grinding the powder in a mortar embedded in dry ice and mulling with toluene; the samples were then spread between precooled Infrasil quartz disks. The $[Cu(HB(3,5\text{-}Ph_2pz)_3)]_2(O_2)$ mineral oil mull samples were prepared at room temperature. The solution samples were prepared by making solutions of known concentration which were dilute enough to prevent precipitation at the experimental temperatures. Liquid methylene chloride solution samples were quickly transferred by a precooled syringe into a 0.50-cm far-UV quartz cell (Wilmad Glass Co.) at the end of a glass tube in the optical cryostat, already equilibrated to the experimental temperature (−30 to −80 °C).

Resonance Raman samples were prepared by grinding the solid material either by itself or with an appropriate amount of KBr or, when an

(10) Jacobson, R. R.; Tyeklár, Z.; Farooq, A.; Karlin, K. D.; Liu, S.; Zubieta, J. *J. Am. Chem. Soc.* **1988**, *110*, 3690–3692.
(11) Freedman, T. B.; Loehr, J. S.; Loehr, T. M. *J. Am. Chem. Soc.* **1976**, *98*, 2809–2815.
(12) Larrabee, J. A.; Spiro, T. G. *J. Am. Chem. Soc.* **1980**, *102*, 4217–4223.
(13) Kitajima, N.; Fujisawa, K.; Moro-oka, Y.; Toriumi, K. *J. Am. Chem. Soc.* **1989**, *111*, 8975–8976.
(14) (a) Ross, P. K.; Solomon, E. I. *J. Am. Chem. Soc.* **1990**, *112*, 5871–5872. (b) Ross, P. K.; Solomon, E. I. *J. Am. Chem. Soc.* **1991**, *113*, 3246–3259.
(15) Kitajima, N.; Koda, T.; Hashimoto, S.; Kitagawa, T.; Moro-oka, Y. *J. Chem. Soc., Chem. Commun.* **1988**, 151–152.
(16) Thompson, J. S. *J. Am. Chem. Soc.* **1984**, *106*, 4057–4059.
(17) Kitajima, N.; Fujisawa, K.; Fujimoto, C.; Moro-oka, Y.; Hashimoto, S.; Kitagawa, T.; Toriumi, K.; Tatsumi, K.; Nakamura, A. *J. Am. Chem. Soc.* **1992**, *114*, 1277–1291.

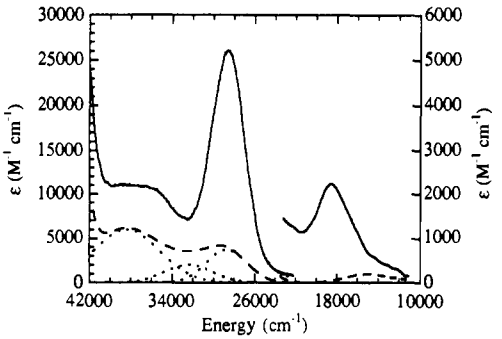

Figure 2. Absorption spectrum of a solution of $[Cu(HB(3,5\text{-}i\text{-}Pr_2pz)_3)]_2(O_2)$ in CH_2Cl_2 at −50 °C (—) and $[Cu(HB(3,5\text{-}i\text{-}Pr_2pz)_3)]_2(\mu\text{-}OH)_2$ in CH_2Cl_2 at room temperature (---). The intensity of the low-energy region corresponds to the right-hand axis. Gaussian resolution of the charge-transfer transitions of $[Cu(HB(3,5\text{-}i\text{-}Pr_2pz)_3)]_2(\mu\text{-}OH)_2$ is shown by the dotted line.

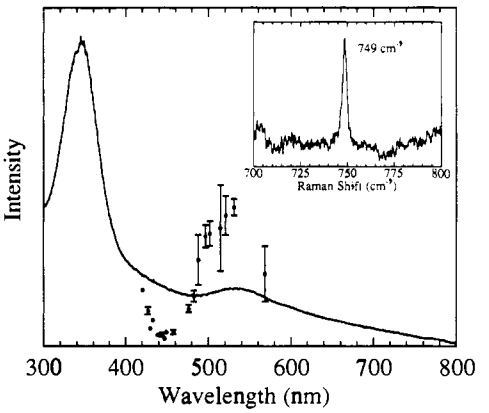

Figure 3. Absorption spectrum of a toluene mull of crystalline $[Cu(HB(3,5\text{-}i\text{-}Pr_2pz)_3)]_2(O_2)$ at 77 K, with the resonance enhancement profile of the 749 cm^{-1} Raman feature. Error bars represent the standard deviation from three or more experiments. Insert: 749 cm^{-1} resonance Raman feature.

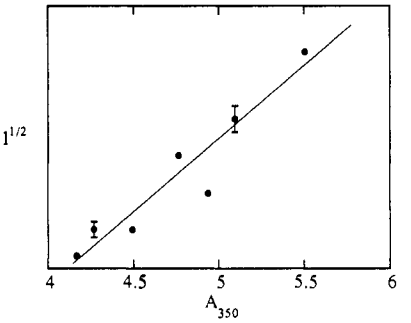

Figure 4. Plot of the square root of the relative intensity of the 749 cm^{-1} Raman peak in $[Cu(HB(3,5\text{-}i\text{-}Pr_2pz)_3)]_2(O_2)$ vs the Shorygin function A (eq 1 in text) for a 350-nm resonant transition. Error bars represent standard deviations for three or more experiments. The Raman intensity data are from the seven highest excitation energy points in Figure 3.

internal standard was used for enhancement profiles, with K_2SO_4, in a mortar embedded in dry ice. The homogeneously mixed solid samples were then put into NMR tubes. The samples were cooled using a nitrogen flow system, which allows liquid nitrogen cooled gas to flow over the sample keeping it at about 110 K, and spun to prevent local heating by the laser. An approximately 180° backscattering geometry was used to collect scattered light from the sample. Resonance Raman spectra were measured using a Spex 1403 double monochromator with a cooled Princeton Applied Research 1455 intensified OMA detector interfaced to a personal computer by a PAR Model 1461 interface. Light sources include a Coherent I-18UV argon ion laser, a Coherent I-90K krypton ion laser, and rhodamine 6G and stilbene 3 dye lasers. Laser power was typically 40 mW or less to prevent photodecomposition of the samples, although at wavelengths below 400 nm rapid photodecomposition was unavoidable. Spectral bandwidths were 2 cm^{-1} for determination of peak positions and typically 4 cm^{-1} for collection of enhancement profile data. The 984 cm^{-1} Raman peak of solid K_2SO_4 was used for calibration of the Raman peak intensities for enhancement profiles.

Infrared absorption spectra were collected from mineral oil mulls between CsI plates (Wilmad Glass Co.) at room temperature. The spectra were taken on an IBM Bruker IR-98 Fourier transform infrared spectrometer.

Magnetic susceptibility measurements were taken on a Quantum Design MPMS superconducting quantum interference device. Measurements were taken with a magnetic field of 10 kG below 50 K and 50 kG above 50 K. Electron paramagnetic resonance spectra were taken on a Bruker ER 220-D-SRC spectrometer using an X-band cavity (~9.4 GHz) at 77 K. Solid powder samples of the mostly diamagnetic material were placed in quartz tubes, and the concentration was determined from the weight and volume of the sample. Standard solutions of 1.00 and 5.00 mM $CuSO_4$ in 1:1 glycerol/water glasses of the same volume as the solid samples were used for spin quantitation.

The normal coordinate analysis was based on a Wilson FG matrix method[18] using a modified Urey-Bradley force field. The calculations were performed on an IBM PC computer using a modified Schachtschneider program.[19]

III. Results and Analysis

A. Spectral Features of Side-on Structure. The absorption spectrum of a methylene chloride solution of $[Cu(HB(3,5\text{-}i\text{-}Pr_2pz)_3)]_2(O_2)$ at −50 °C in Figure 2 shows absorption bands at 350 (28 600 cm^{-1}, ϵ = 26 000 M^{-1} cm^{-1}) and 538 nm (18 600 cm^{-1}, ϵ = 2000 M^{-1} cm^{-1}), a broad feature at about 260 nm (~38 000 cm^{-1}), and weak features on the low-energy side of the 538-nm band which are at an appropriate energy to be assigned as ligand field transitions of the square pyramidal coppers. A mull spectrum of the structurally characterized crystalline material is shown in Figure 3. Light scattering by the mull distorts the relative intensities of the absorption bands. However, both of the intense features in the solution absorption spectrum above 300 nm are present in the spectrum of the crystalline solid, indicating that the absorption spectrum is intrinsic to the side-on bridged structure and not the result of an equilibrium mixture of chromophores in solution. The absorption spectrum of the bis-μ-OH complex, $[Cu(HB(3,5\text{-}i\text{-}Pr_2pz)_3)]_2(\mu\text{-}OH)_2$, is shown as the dashed line in Figure 2 for comparison with the peroxide-bridged complex. At energies below 25 000 cm^{-1}, only a weak feature at about 675 nm (14 800 cm^{-1}, ϵ = 200 M^{-1} cm^{-1}) is observed, which is consistent with the ligand field transitions of tetragonal cupric complexes and corresponds to the low-energy shoulder of the 538-nm band of the peroxide complex. Three absorption bands in the 250–450 nm region are resolved by a Gaussian analysis. One band is centered at 348 nm (28 720 cm^{-1}, ϵ = 3700 M^{-1} cm^{-1}), a second at 310 nm (32 400 cm^{-1}, ϵ = 2000 M^{-1} cm^{-1}), and a third at 260 nm (38 400 cm^{-1}, ϵ = 6500 M^{-1} cm^{-1}). The 260-nm band is at an energy where the pyrazole (π_2) → Cu charge transfer is expected[20] and corresponds to the band at the same energy in the spectrum of the peroxide complex. The 348- and 310-nm bands are each in the appropriate energy region to be assigned to either an OH → Cu charge transfer or a pyrazole (π_1) → Cu charge-transfer transition.[20] The 350-nm band in the peroxide complex is greater than 5-fold more intense than either of these two bands in the bis-μ-OH spectrum.

In addition, the resonance Raman spectrum of the crystalline solid has a strong peak at 749 cm^{-1} (shown as an insert in Figure 3), which is at nearly the same energy as the O–O stretch for the solution. The frequency of this vibrational mode and its shift upon

(18) (a) McIntosh, D. F.; Michaelian, K. H. *Can. J. Spectrosc.* **1979**, *24*, 1–10. (b) McIntosh, D. F.; Michaelian, K. H. *Can. J. Spectrosc.* **1979**, *24*, 35–40. (c) McIntosh, D. F.; Michaelian, K. H. *Can. J. Spectrosc.* **1979**, *24*, 65–74.

(19) (a) Schachtschneider, J. H. Technical Report No. 57-65, Shell Development Co., Emeryville, CA, 1966. (b) Fuhrer, H.; Kartha, V. B.; Kidd, K. G.; Kreuger, P. J.; Mantsch, H. H. *Computer Programs for Infrared Spectroscopy*; Bulletin No. 15; National Research Council of Canada: Ottawa, 1976.

(20) Schugar, H. J. In *Copper Coordination Chemistry: Biochemical and Inorganic Perspectives*; Karlin, K. D., Zubieta, J., Eds.; Adenine Press: New York, 1983; pp 43–74.

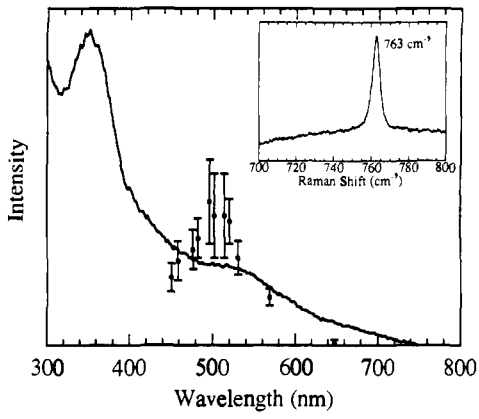

Figure 5. Absorption spectrum of a mineral oil mull of $[Cu(HB(3,5\text{-}Ph_2pz)_3)]_2(O_2)$ at 77 K, with the resonance enhancement profile of the 763 cm^{-1} Raman feature. Error bars represent the standard deviation for three or more experiments.

isotopic substitution of peroxide [vide infra] identify it as a peroxide stretch, consistent with the 1.4 Å O–O bond length in the crystal structure.[13] The resonance enhancement profile in Figure 3 for the ν(O–O) Raman feature shows that it is enhanced by both absorption features. The profile peaks with the visible absorption maximum and increases toward the UV absorption maximum until photodecomposition prevents data collection at lower wavelengths. The linearity of the plot in Figure 4 of the square root of the normalized Raman intensity, $I^{1/2}$, versus the Shorygin function A_{ν_0},[21] where ν_0 is the Raman excitation frequency and ν_e is the assumed frequency of the resonant transition shows that the observed preresonance enhancement is associated with the 350-nm absorption band. The bands at 350 and 538

$$A_{\nu_0} = [(1 + (\nu_0/\nu_e)^2)]/[1 - (\nu_0/\nu_e)^2]^2 \quad (1)$$

nm in the absorption spectrum of $[Cu(HB(3,5\text{-}i\text{-}Pr_2pz)_3)]_2(O_2)$ are thus assigned as peroxide-to-copper charge-transfer transitions of the structurally characterized side-on peroxide-bridged copper dimer.

A complex similar to $[Cu(HB(3,5\text{-}i\text{-}Pr_2pz)_3)]_2(O_2)$, but with R = Ph instead of R = *i*-Pr,[17] was also studied. Due to its greater thermal stability and easier preparation of isotopically substituted analogues, some of the experiments presented below were performed on this complex rather than the R = *i*-Pr complex; however, many of the experiments were performed on both complexes. This complex has not been structurally characterized by X-ray crystallography; however, its spectroscopic features are nearly identical to those of the structurally characterized R = *i*-Pr complex.[17] A mull spectrum of $[Cu(HB(3,5\text{-}Ph_2pz)_3)]_2(O_2)$ (Figure 5) contains the same absorption features as found for $[Cu(HB(3,5\text{-}i\text{-}Pr_2pz)_3)]_2(O_2)$. In addition, a resonance Raman feature corresponding to ν(O–O) is observed at 763 cm^{-1} (based on its shift upon isotopic perturbation; vide infra) and is also enhanced by the visible absorption band, as shown by the resonance enhancement profile in Figure 5. Photodecomposition of this complex at wavelengths below 440 nm prevents collection of profile data into the UV absorption band.

B. Magnetic Susceptibility. Temperature-dependent magnetic susceptibility measurements were taken for $[Cu(HB(3,5\text{-}Ph_2pz)_3)]_2(O_2)$. Quantitation of the Curie law behavior of the low-field, low-temperature data (2 K < T < 50 K, 10 kG) shows that <1% of the sample is present as a paramagnetic impurity, while the complex itself is diamagnetic. Spin quantitation[22] of a $g \approx 2$ signal in the electron paramagnetic resonance (EPR) spectrum shows that this signal is due to <1% of the Cu(II) in the sample. The molar susceptibility at 50 kG between 100 and 250 K, above which thermal decomposition of the sample occurs, is plotted in Figure 6. Also plotted are theoretical susceptibilities[23]

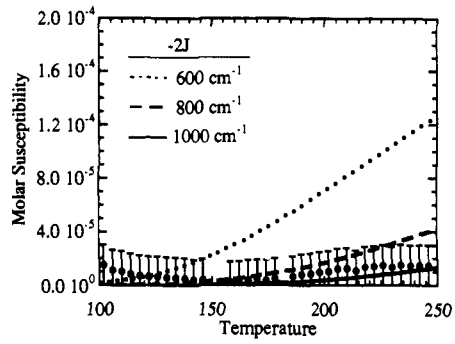

Figure 6. Plot of molar susceptibility vs temperature, 100 K < T < 250 K, for $[Cu(HB(3,5\text{-}Ph_2pz)_3)]_2(O_2)$ (●) and theoretical plots for $-2J$ = 600 cm^{-1} (···), $-2J$ = 800 cm^{-1} (- - -), and $-2J$ = 1000 cm^{-1} (—). Error bars represent the scatter in the data from four different experiments.

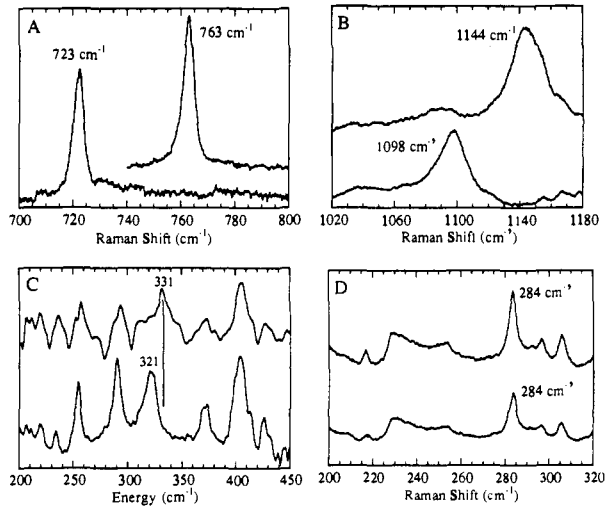

Figure 7. Vibrational data for Cu_2O_2 core of $[Cu(HB(3,5\text{-}Ph_2pz)_3)]_2(O_2)$: (A) resonance Raman spectrum of 763 cm^{-1} peak; (B) resonance Raman spectrum of 1144 cm^{-1} peak; (C) infrared spectrum of 331 cm^{-1} peak; (D) resonance Raman spectrum of 284 cm^{-1} peak. For each panel, the $^{16}O_2$ spectrum is on top, and the $^{18}O_2$ spectrum is on the bottom.

for singlet–triplet splittings of $-2J$ = 600, 800, and 1000 cm^{-1}. This plot shows that a splitting of $-2J$ = 1000 cm^{-1} would not be distinguishable from the scatter in the data. However, a splitting of 800 cm^{-1} would produce an increase in susceptibility at the higher measured temperatures which would be distinguishable above the error bars taken from the scatter in the data from several experiments. No increase in susceptibility is observed, indicating that strong antiferromagnetic coupling of the cupric ions occurs, with $-2J$ > 800 cm^{-1}.

C. Vibrational Studies and Normal Coordinate Analysis. Three features which shift to lower frequency upon isotopic substitution of oxygen have been identified in the vibrational spectra of $[Cu(HB(3,5\text{-}Ph_2pz)_3)]_2(O_2)$. A peak is seen in the resonance Raman spectrum in Figure 7A at 763 cm^{-1} which shifts to 723 cm^{-1} upon isotopic substitution of $^{16}O_2$ by $^{18}O_2$, allowing its assignment as the intraperoxide stretch, ν(O–O). A broad peak is observed in the resonance Raman spectrum at 1144 cm^{-1}, shifting to 1098 cm^{-1} upon isotopic substitution, as shown in Figure 7B. Peaks corresponding to these are observed in the resonance Raman spectra of $[Cu(HB(3,5\text{-}i\text{-}Pr_2pz)_3)]_2(^{16}O_2)$ at 749 and 1055 cm^{-1}. A peak is also observed at 331 cm^{-1} in the infrared absorption spectrum of $[Cu(HB(3,5\text{-}Ph_2pz)_3)]_2(^{16}O_2)$ which is seen in Figure 7C to shift to 321 cm^{-1} upon isotopic substitution. No other peaks which shift upon isotopic substitution were found in the infrared spectrum between 200 and 1000 cm^{-1}. The 1144 cm^{-1} peak is too high in frequency to be reasonably fit as a fundamental in a normal coordinate analysis, so it is assigned as an overtone of

(21) Clark, R. J. H.; Mitchell, P. D. *J. Mol. Spectrosc.* **1974**, *51*, 458–474.
(22) Aasa, R.; Vänngard, T. *J. Magn. Reson.* **1975**, *19*, 308–315.
(23) Carlin, R. L. *Magnetochemistry*; Springer-Verlag: New York, 1986.

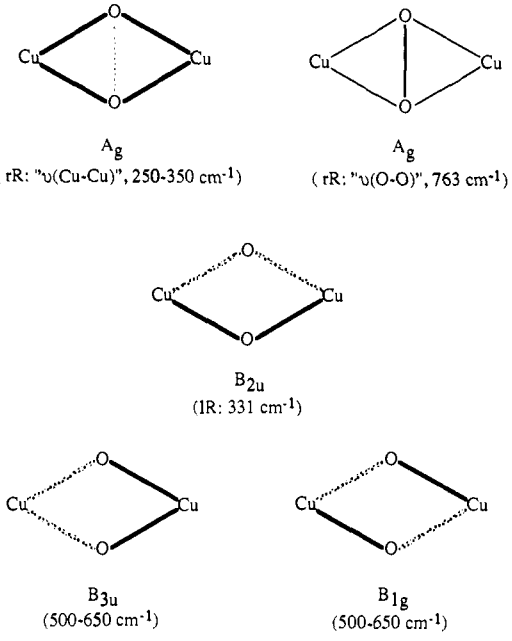

Figure 8. Depictions of the in-plane normal vibrational modes of the side-on peroxide-bridged copper dimer. Broken lines increase in length as solid lines decrease in length. Bonds which do not change in length during a given vibration are not shown. Thicker lines indicate the dominant motion in the two A_g modes.

a non-totally symmetric fundamental at about 572 cm^{-1}. This assignment is consistent with the assignment by Sanders-Loehr et al.[24] of peaks observed at 545 and 1080 cm^{-1} which shift to lower frequency upon isotopic substitution in the resonance Raman spectrum of oxyhemocyanin. The 1080 cm^{-1} peak in oxyhemocyanin is significantly more intense than the 545 cm^{-1} peak, due to the fact that the first overtone is totally symmetric and may therefore show *A*-term resonance enhancement, while a non-totally symmetric fundamental will not.[25] No peak near one-half the frequency of the 1144 cm^{-1} peak is observed to shift upon isotopic substitution in the resonance Raman spectrum of $[Cu(HB(3,5\text{-}Ph_2pz)_3)]_2(O_2)$. The intensity of the 545 cm^{-1} peak in the oxyhemocyanin spectrum is probably due to the lack of rigorous symmetry in the protein site, while this complex is centrosymmetric.

A preliminary normal coordinate analysis was performed fitting the 763 and 331 cm^{-1} vibrations and their isotope shifts to a D_{2h} (x axis = Cu–Cu, z perpendicular to Cu_2O_2 plane) side-on peroxide-bridged copper dimer using the bond lengths from the X-ray crystal structure of $[Cu(HB(3,5\text{-}i\text{-}Pr_2pz)_3)]_2(O_2)$.[13] The 763 cm^{-1} peak was assigned as an A_g vibration involving mostly a change in O–O bond length, and the 331 cm^{-1} peak was assigned as a B_{2u} vibration. The calculation also predicted two non-totally symmetric vibrations between 500 and 650 cm^{-1} of B_{1g} and B_{3u} symmetry, one of which must correspond to the fundamental of the 1144 cm^{-1} overtone. In addition, a second A_g peak was predicted between 250 and 350 cm^{-1} with an isotopic shift of less than 0.5 cm^{-1}. This totally symmetric vibration would be expected to have significant resonance Raman intensity, and a very strong peak (strongly resonance enhanced by the 350-nm band; vide infra) is observed at 284 cm^{-1} in $[Cu(HB(3,5\text{-}Ph_2pz)_3)]_2(O_2)$, with <0.5 cm^{-1} shift upon isotopic substitution (Figure 7D). A corresponding peak is seen at 285 cm^{-1} in $[Cu(HB(3,5\text{-}i\text{-}Pr_2pz)_3)]_2(O_2)$.

In order to correlate the low O–O stretching frequency in the side-on structure to bond strength, it is important to perform a complete normal coordinate analysis of the vibrational data. This is because the significant mechanical interactions of the closed ring system may greatly perturb the vibrational frequencies independent of any change in force constants of the bonds. A normal coordinate analysis was performed using the structural parameters from the X-ray crystal structure of $[Cu(HB(3,5\text{-}i\text{-}Pr_2pz)_3)]_2(O_2)$[13] and the data for the four vibrations identified in $[Cu(HB(3,5\text{-}Ph_2pz)_3)]_2(O_2)$. The five in-plane vibrational modes of the Cu_2O_2 unit, which have A_g, A_g, B_{1g}, B_{2u}, and B_{3u} symmetry, were included in a modified Urey-Bradley force field. These normal modes are shown in Figure 8. The normal coordinate calculations are consistent with the above assignments of the 763, 331, and 284 cm^{-1} vibrations, but they could be refined by assigning the 572 cm^{-1} fundamental associated with the 1144 cm^{-1} peak in the resonance Raman spectrum to either the B_{1g} or B_{3u} mode. The sets of force constants to which the vibrational frequencies are best fit for each assignment of the 572 cm^{-1} mode are given in Table IA,B. In both cases, the B_{1g} mode has a higher frequency than the B_{3u} mode, so that for the case in Table IA in which the B_{1g} mode is placed at 572 cm^{-1}, the Cu–O force constant is lower (1.42 mdyn/Å) than for the case in Table IB in which the B_{3u} mode is placed at 572 cm^{-1} (1.72 mdyn/Å). In both cases, however, the O–O force constant is found to be between 2.4 and 2.5 mdyn/Å. This is significantly lower than the O–O force constants which we derived previously for the end-on monomer (2.9 mdyn/Å) and trans end-on dimer (3.1 mdyn/Å) complexes,[9] also using a Urey-Bradley force field and a similar force constant basis set. The quadratic force constant has been shown to correlate well with bond length in diatomic and small polyatomic molecules,[26] for which the bond length is determined primarily by bond strength in comparing bonds between similar atoms. The lower force constant therefore shows that the side-on bridged complex studied here has a weaker O–O bond than the end-on monomer or dimer. Combined with the greater σ donation from the peroxide π^* orbitals in the side-on complex (see section D), this must be a result of the interaction of the unoccupied peroxide σ^* orbital with the HOMO in the side-on complex which was predicted by the Xα calculations[14] described in the Introduction. This interaction involves back-bonding of a small amount of electron density into the highly antibonding σ^* orbital of the peroxide, thus resulting in the weaker O–O bond.

It was found in the case of the end-on monomer and dimer normal coordinate calculations[9] that, while the choice of interaction force constants and values for unavailable vibrational frequencies significantly affected the Cu–O force constants, these choices had little effect on the values calculated for the O–O force constants. In order to take into account any effects of the greater mechanical interactions expected for the side-on structure, we systematically studied the sensitivity of the calculations for the side-on complex to perturbations in the model. The calculations show that all of

Table I. Normal Coordinate Analysis of Side-on Bridged Complex

normal mode[a]	obsd frequencies (cm^{-1}) $^{16}O_2$	obsd frequencies (cm^{-1}) $^{18}O_2$	calcd frequencies (cm^{-1}) $^{16}O_2$	calcd frequencies (cm^{-1}) $^{18}O_2$	force const (mdyn/Å)
A. Calculations for B_{1g} = 572 cm^{-1}					
A_g	763	723	764.7	721.2	k_{O-O} = 2.43
B_{1g}	572[b]	549[b]	573.8	547.7	k_{Cu-O} = 1.42
B_{3u}			523.7	494.9	
B_{2u}	331	321	333.4	318.2	0.41 (0.15)[c]
A_g	284	284	284.0	283.9	0.26 (−0.12)[d]
B. Calculations for B_{3u} = 572 cm^{-1}					
A_g	763	723	764.5	721.3	k_{O-O} = 2.45
B_{1g}			629.9	601.3	k_{Cu-O} = 1.72
B_{3u}	572[b]	549[b]	575.3	543.7	
B_{2u}	331	321	333.5	318.3	0.37 (0.04)[c]
A_g	284	284	284.2	284.0	0.28 (−0.14)[d]

[a] Symmetries are given for the D_{2h} point group. [b] Half of the frequency of the observed first overtone. [c] Cu–O–Cu bend force constant (interaction force constant in parentheses). [d] O–Cu–O bend force constant (interaction force constant in parentheses).

(24) Sanders-Loehr, J.; Loehr, T. M.; Ling, J.; Sharma, K. D.; Nestor, L. M.; Czernuscewicz, R.; Spiro, T. G. Manuscript in preparation. Personal communication from J. Sanders-Loehr.

(25) Clark, R. J. H.; Stewart, B. In *Structure and Bonding*; Dunitz, J. D., et al., Eds.; Springer-Verlag: Berlin, 1979; Vol. 36, pp 1–80.

(26) Hershbach, D. E.; Laurie, V. W. *J. Chem. Phys.* **1961**, *35*, 458–463.

the O–O motion is distributed between the two A_g modes, with >90% in the 763 cm^{-1} mode, while the 284 cm^{-1} vibration is mostly copper motion. In order to determine whether an increased effective copper mass due to other ligands not included in the Cu_2O_2 model would have any significant effects, the copper mass was increased from 63 to 500 amu. Using the same force constants, the ^{500}Cu calculations yielded a similar frequency for the higher energy (763 cm^{-1}) A_g mode, although the lower energy A_g mode dropped to about 100 cm^{-1}. A fit to all of the frequencies using the high Cu mass did not yield reasonable results. A more reasonable estimate of the effective mass of the copper was obtained using a copper mass of 63, but adding two "ligands" with a mass of 50 amu 2.0 Å away from each copper, opposite the peroxide oxygens. This calculation brought the lower energy A_g mode back up to an energy consistent with our assignment of the 284 cm^{-1} peak, and the higher energy A_g mode still had a frequency of about 763 cm^{-1} with an O–O force constant of 2.4 mdyn/Å. In all of these calculations, the $^{16}O_2 \rightarrow {}^{18}O_2$ isotope shift of the 284 cm^{-1} mode remained <0.5 cm^{-1}. The parameters which most greatly affected the calculated value of the O–O force constant, k_{O-O}, were the force constant of the O–Cu–O bend and the corresponding interaction force constant (the last force constants listed in Table IA,B). We therefore fixed all other force constants and varied k_{O-O} to explore how large it could become and still fit the vibrational data. With k_{O-O} equal to or greater than that of the monomer (2.9 mdyn/Å),[9] the interaction force constant becomes much larger (≥0.4 mdyn/Å) than the corresponding bending force constant, which is not reasonable. Thus, the k_{O-O} for the side-on bridged dimer must be lower than k_{O-O} for the end-on bridged dimer (3.1 mdyn/Å)[9] and monomer.

D. Excited-State Spectral Assignments. The two absorption features at 350 and 538 nm in Figures 2 and 3, shown above to be peroxide-to-copper charge-transfer transitions of the Cu_2O_2 chromophore in $[Cu(HB(3,5\text{-}i\text{-}Pr_2pz)_3)]_2(O_2)$, are assigned as the spin- and electric dipole-allowed transitions from $O_2^{2-}(\pi^*_\sigma) \rightarrow Cu(d_{x^2-y^2})$ and $O_2^{2-}(\pi^*_v) \rightarrow Cu(d_{x^2-y^2})$. Each of these CT transitions from the monomer is split into four components by dimer interactions. Figure 9 is a diagram of the ground and excited states involved in these transitions of the side-on bridged dimer (right), the broken-symmetry SCF-Xα-SW calculations[14] (center), and the copper–peroxide monomer (left). Although the π^*_v transition observed at 18 600 cm^{-1} in the side-on dimer is within about 10% of the energy predicted by broken-symmetry SCF-Xα-SW calculations,[14] the π^*_σ transition is predicted to be as much as twice as high in energy as observed. This difference is due to the fact that the broken-symmetry Xα calculations average the four components, which are expected to have much larger splittings for the π^*_σ excited state than for the π^*_v excited state. The four components of each dimer excited state are due to a singlet–triplet splitting ($-2J_{es}$) and a splitting of the symmetric and antisymmetric combinations of the excitation on each half of the dimer. The excited-state singlet–triplet splitting is due to the exchange interaction of the two unpaired electrons, which will be in orbitals which have direct overlap in the CT excited state. This excited-state singlet–triplet splitting may be much greater than the ground-state singlet–triplet splitting ($-2J$ > 800 cm^{-1}; vide supra), since the ground-state interaction must be mediated through a superexchange pathway. In the study on the end-on dimer,[9] the antiferromagnetic excited-state singlet–triplet splitting of the π^*_v transition was found to be about 8000 cm^{-1}. The singlet–triplet splitting of the π^*_σ transition in this complex is expected to be much larger, since the intensities of the absorption bands show much greater overlap of the relevant orbitals (vide infra). This should lower the energy of the observed (singlet) transition well below that calculated for the average of the four components.

In the dimer, there are two possible transitions from each π^* orbital for each spin state, one to each copper. The full symmetry of the dimer requires symmetric and antisymmetric combinations of these transitions. The splitting of the symmetric combination (A_g for π^*_σ and B_{2g} for π^*_v in Figure 9), which is electric dipole forbidden in the centrosymmetric complex due to cancellation of the transition vectors, and the antisymmetric combination (B_{3u} for π^*_σ and B_{1u} for π^*_v in Figure 9), which is electric dipole allowed due to constructive addition of the transition vectors, is mediated by excitation transfer between the two sides of the dimer. There are both Coulombic and exchange contributions to this g/u splitting. The Coulombic contribution, the i term in Figure 9, is derived from dipole interactions between transition moments, while the exchange contribution, the L term in Figure 9, involves electron transfer between the two halves of the dimer. The Coulombic contribution may be estimated by a simple dipole–dipole approximation:[27]

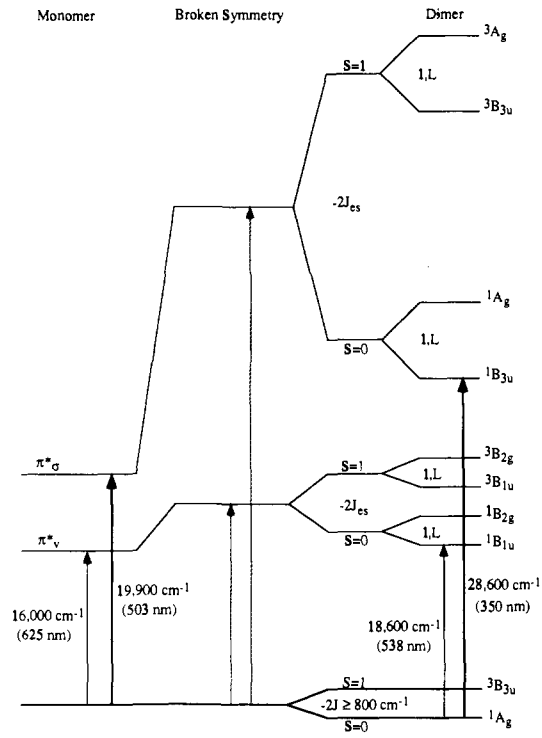

Figure 9. Excited-state splitting diagram for the peroxide-to-copper CT excited states in the side-on bridged dimer (right) compared to the broken-symmetry Xα calculated states (center) and the monomer complex (left). Arrows indicate observed transitions in the model complexes (solid) and calculated broken-symmetry transitions (broken). Thicker arrows represent greater observed intensity. Splitting terms are as described in the text.

$$\Delta E(u\text{-}g) = 2|M|^2(1 - 3\cos^2\theta)/R^3 \quad (2)$$

where M is the transition moment, R is the center-to-center distance between dipoles, and θ is the angle between each dipole and the dipole–dipole axis ($\theta = 0°$ for π^*_σ and 90° for π^*_v). For π^*_σ, this places the A_g component about 50 000 cm^{-1} above the electric dipole-allowed B_{3u} component, while for π^*_v the B_{2g} component is placed about 2000 cm^{-1} below the electic dipole-allowed B_{1u} component. This is likely a poor estimate of the g/u splitting, however, as the exchange contribution, which is related to the HOMO/LUMO splitting of the valence orbitals on the two coppers, may dominate.[28] For the side-on bridged complex, this further lowers the energy of the $^1B_{3u}$ component of π^*_σ in Figure 9 relative to the ^1A_g component.

The integrated intensities of the peroxide-to-copper and charge-transfer absorption bands provide important information about peroxide–copper bonding and allow a quantitative comparison of the differences in bonding between the side-on dimer, the trans end-on dimer, and the monomer. In general, the σ donor strength of a ligand can be estimated from CT intensities, providing that the molecular orbitals involved in the bonding of the ligand to the metal ion are the donor and acceptor orbitals involved in the CT process. This should be the case for low-energy intense

(27) Kasha, M.; Rawls, H. R.; El-Bayoumi, M. A. *Pure Appl. Chem.* **1965**, *11*, 371–392.
(28) Tuczek, F.; Solomon, E. I. Manuscript in preparation.

CT transitions as in the copper–peroxide complexes. The oscillator strength, f, in eq 3a,b relates the integrated intensity of an absorption band to the transition moment integral:

$$f_{exp} = (4.32 \times 10^{-9}) \int \epsilon(\nu)\, d\nu \quad (3a)$$

$$f_{theory} = (8\pi^2 mc/3h)\nu \left[\int \psi^g \mathbf{M} \psi^e \, d\tau \right]^2 \quad (3b)$$

In eq 3a, ϵ is the molar extinction coefficient (M^{-1} cm^{-1}) and ν is the frequency in cm^{-1}. In eq 3b, $[\int \psi^g \mathbf{M} \psi^e \, d\tau]$ is the transition moment integral in cm, ψ^g and ψ^e are the ground and excited states involved in the transition, and $(8\pi^2 mc/3h) = 1.085 \times 10^{11}$ cm^{-1}. For a copper peroxide monomer, the CT transition involves excitation from a predominantly ligand O_2^{2-} (π^*_σ) donor orbital, ψ^D, to a predominantly Cu($d_{x^2-y^2}$) half-occupied acceptor orbital, ψ^A. The CT donor and acceptor orbitals can be expressed as linear combinations of metal, χ_M, and ligand, χ_L, orbitals:

$$\psi^D = C^D_M \chi^D_M + C^D_L \chi^D_L \quad (4a)$$

$$\psi^A = C^A_M \chi^A_M + C^A_L \chi^A_L \quad (4b)$$

In the electric dipole approximation, the transition moment integral for the CT transition from ψ^D to ψ^A contains the four terms given by[29]

$$\int \psi^D \mathbf{r} \psi^A \, d\tau = C^D_M C^A_M \int \chi^D_M \mathbf{r} \chi^A_M \, d\tau + C^D_M C^A_L \int \chi^D_M \mathbf{r} \chi^A_L \, d\tau + C^D_L C^A_M \int \chi^D_L \mathbf{r} \chi^A_M \, d\tau + C^D_L C^A_L \int \chi^D_L \mathbf{r} \chi^A_L \, d\tau \quad (5)$$

While all of the terms will be similarly related to the overlap of the metal and ligand orbitals, calculations[30] have shown that the ligand–ligand term (the last term in eq 5) dominates the intensity of charge-transfer transitions. Note that χ_L will contain terms from all ligands, not just peroxide. However, in the predominantly peroxide π^*_σ donor orbital, contributions to χ^D_L from ligands other than peroxide will be negligible as demonstrated in Xα calculations.[14] Therefore, although orbitals from ligands other than peroxide may contribute to χ^A_L, they will have little effect on the transition moment integral due to lack of overlap with χ^D_L. The ligand–ligand term in eq 5 reduces to $C^D_L C^A_L \vec{r}$,[29] where $\vec{r}$ is the vector from the bound oxygen of the peroxide to the metal, so that the transition moment is

$$\left[\int \psi^g \mathbf{M} \psi^e \, d\tau \right]^2 \approx (C^D_L C^A_L \vec{r})^2 \quad (6)$$

As only ψ^D and ψ^A have appreciable peroxide π^*_σ character, $(C^D_L)^2 = (1 - (C^A_L)^2)$. Substituting this into eq 6 and the resulting expression into eq 3b gives eq 7, which can be used to estimate the amount of peroxide character in the half-occupied HOMO for small values of $(C^A_L)^2$. For dimers, the ligand–ligand term

$$f_{exp}/[(1.085 \times 10^{11})\nu r^2] = (C^A_L)^2(1 - (C^A_L)^2) \approx (C^A_L)^2 \quad (7)$$

in eq 5 reduces to $(C^D_L C^A_L \vec{r} \cos\phi)$,[29] where ϕ is the angle between the transition vectors to each copper in the dimer. These vectors are taken to be from the center of the O–O bond to the copper in the dimers. Thus, for the side-on and trans end-on dimers in which the transition vectors are from the center of symmetry to the coppers, $\cos\phi = 1$, and all of the transition intensity is associated with the observed electric dipole-allowed component. For the cis end-on structure, ϕ depends on the Cu–Cu, Cu–O, and O–O distances.

The σ donor ability of the peroxide corresponds to the amount of Cu($d_{x^2-y^2}$) character in the fully occupied, predominantly peroxide π^*_σ orbitals, which is given by $(C^D_M)^2$. Since ψ^D has only Cu($d_{x^2-y^2}$) and $O_2^{2-}(\pi^*_\sigma)$ character, the σ donor ability may be estimated using $(C^D_M)^2 = (1 - (C^D_L)^2) = (C^A_L)^2$. Thus eq 7 directly relates the σ donation by the peroxide π^*_σ orbitals to the intensities of the peroxide-to-copper charge-transfer transitions.

Table II. Parameters Used To Derive Ratio of $(C^D_M)^2$

complex	f_{total}[a]	f/ν (10^3 Å)[b]	r^2 (Å^2)	$(C^D_L)^2$ ratio
monomer	0.105	0.537	3.61	1
end-on dimer	0.252	1.35	4.75	1.9
side-on dimer	0.479	1.73	3.17	3.7
oxyHc (side-on)[c]	0.488	1.73	3.17	3.7
oxyHc (cis-μ-1,2)[d]	0.488	1.73	3.25[e]	3.6

[a] Oscillator strength from integrated intensity of all observed peroxide-to-copper charge-transfer transitions. [b] Sum of oscillator strengths of each peroxide-to-copper charge-transfer transition divided by its frequency at ϵ_{max}. [c] Assumes same Cu_2O_2 structure as $[Cu(HB(3,5\text{-}i\text{-}Pr_2pz)_3)]_2(O_2)$. [d] Assumes a planar end-on cis-μ-1,2 structure with Cu–Cu = 3.6 Å, O–O = 1.42 Å, Cu–O = 1.9 Å, giving $\phi = 41°$. [e] $r^2 \cos\phi^2$, since in the noncentrosymmetric dimer the transition dipoles to each copper are not parallel and the intensity of the π^*_σ transition is distributed between two electric dipole-allowed components (see text).

Using the above method and the integrated intensities and average frequencies determined experimentally from the absorption spectra of the monomer, end-on dimer, and side-on dimer complexes, a ratio of charge donation from the peroxide to the metal of 1:1.9:3.7 is obtained for this series. (Table II gives the parameters used to obtain these ratios.) This indicates that the peroxide donates approximately twice the electron density (or roughly the same amount per copper) to two end-on bound coppers as to one. The side-on bridging peroxide donates nearly 4 times as much electron density to the coppers as compared to the monomer, or about twice as much per copper as either end-on complex. This is due to the fact that the peroxide occupies two coordination positions per copper in the side-on bridged complex. This produces a less negative peroxide in the side-on bridged dimer than in the end-on bridged dimer, which is less negative than the monomer. The broken-symmetry Xα calculations[14] predicted this less negative peroxide in the side-on bound complex. The calculated ratio of the peroxide character in the LUMO (the orbital involved in the antibonding interaction with $O_2^{2-}(\pi^*_\sigma)$ and the acceptor orbital in the CT transition in the dimers) for the side-on and end-on complexes is between 2:1 and 3:2, depending upon the copper sphere radius chosen for the calculation, in good agreement with our experimentally derived values. The side-on bridging peroxide may therefore be described as less negative and thus more "superoxide-like" than the peroxides in the end-on complexes. This would be expected to result in a stronger O–O bond; however, this is not the case as shown by the normal coordinate analysis in part C. The weaker O–O bond in a less negative peroxide confirms the importance of the role of the peroxide σ^* orbital in the HOMO of the side-on complex and confirms that in this complex the peroxide must be considered as a π acceptor ligand.

It is important to note that the relative $(C^D_M)^2$ derived for *Busycon canaliculatum* oxyhemocyanin is 3.7 times that of the monomer if the side-on bridging geometry is assumed and 3.6 if a planar end-on cis-μ-1,2 geometry is assumed. The number derived for the cis-μ-1,2 model takes into account the approximately 41° angle between the transition vectors expected for the cis structure. This causes both components of the π^*_σ transition to be electric dipole allowed, so that only 57% of the intensity of the π^*_σ-to-Cu CT would be associated with the transition observed at 345 nm. These values derived for oxyhemocyanin, which are much larger than for the end-on dimer but nearly the same as for the side-on dimer, will be further considered in the Discussion section.

The enhancement profiles of the resonance Raman peaks provide details about the excited-state distortions which result from the peroxide-to-copper charge-transfer transitions. The 749 cm^{-1} peak of $[Cu(HB(3,5\text{-}i\text{-}Pr_2pz)_3)]_2(O_2)$ was shown in Figures 3 and 4 to be enhanced by both the π^*_σ and π^*_v transitions. The profile of the 285 cm^{-1} Raman peak in Figure 10 and a plot of the square root of its intensity vs the Shorygin function (eq 1) in Figure 11 show that it is not significantly enhanced by the π^*_v transition, but that it is much more strongly enhanced by the 350-nm transition than is the 749 cm^{-1} peak. In the most common *A*-term

(29) Solomon, E. I. *Comments Inorg. Chem.* **1984**, *3*, 225–320.
(30) (a) Ros, P.; Schuit, G. C. A. *Theoret. Chim. Acta (Berlin)* **1966**, *4*, 1–12. (b) Van der Avoird, A.; Ros, P. *Theoret. Chim. Acta (Berlin)* **1966**, *4*, 13–21.

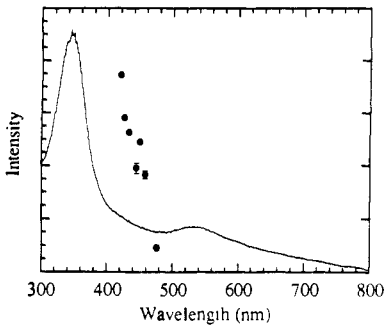

Figure 10. Resonance enhancement profile of 285 cm^{-1} Raman peak vs absorption spectrum of a mull of $[Cu(HB(3,5\text{-}i\text{-}Pr_2pz)_3)]_2(O_2)$. Error bars represent the standard deviation from three or more experiments.

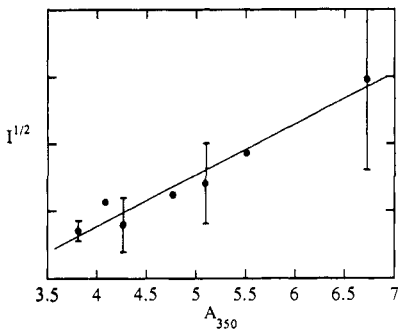

Figure 11. Plot of the square root of the relative intensity of the 285 cm^{-1} Raman peak in $[Cu(HB(3,5\text{-}i\text{-}Pr_2pz)_3)]_2(O_2)$ vs the Shorygin function A (eq 1 in the text) for a 350-nm resonant transition. Error bars represent standard deviations for three or more experiments.

mechanism,[25] resonance Raman peak intensities are enhanced proportionally to the square of the resonant excited-state distortion of the nuclei along the normal mode corresponding to the Raman peak and proportionally to the square of the molar extinction coefficient, ϵ, of the resonant transition. Since nondegenerate excited states may distort only along totally symmetric normal modes, only the A_g modes will be resonance enhanced. The 763 and 284 cm^{-1} peaks (749 and 285 cm^{-1} in the R = *i*-Pr complex) represent the only two A_g fundamentals in the Cu_2O_2 unit; however, the first overtone of a non-totally symmetric mode at 1144 cm^{-1} also shows some enhancement by the π^*_σ transition, since this overtone is totally symmetric. The normal coordinate analysis showed that the 763 cm^{-1} mode is mostly an O–O stretch, while the 284 cm^{-1} mode is mostly a change in the copper–copper distance, as shown in Figure 8. Both the π^*_σ and π^*_v transitions remove antibonding electron density from the O–O region, thus distorting this bond. The lower relative enhancement of the O–O stretching mode by the π^*_σ transition than by the π^*_v transition (compared to ϵ^2 of the absorption bands) indicates that the O–O bond is less distorted by the π^*_σ transition. This is due to the fact that more electron density has already been donated from the π^*_σ orbital than from the π^*_v orbital to the Cu–O bond in the ground state. Thus the π^*_v orbital has more antibonding electron density in the O–O region and a relatively greater bonding change upon excitation. This behavior is similar to that observed for both the monomer[8] and the end-on dimer.[9] The 285 cm^{-1} peak, on the other hand, is much more strongly enhanced by the π^*_σ transition than by the π^*_v transition. This is due to the fact that this transition is from a molecular orbital which is strongly bonding in the ground state to one which is strongly antibonding in the excited state for all four Cu–O bonds (vide infra). Thus, all four Cu–O bonds stretch simultaneously upon excitation, causing dominant distortion along the Cu–Cu vector (i.e., the "ν(Cu–Cu)" A_g mode in Figure 8).

IV. Discussion

A. Electronic Structure of Side-on and End-on Peroxide-Bridged Models. The studies presented here provide significant experimental insight into the unique electronic and vibrational structure

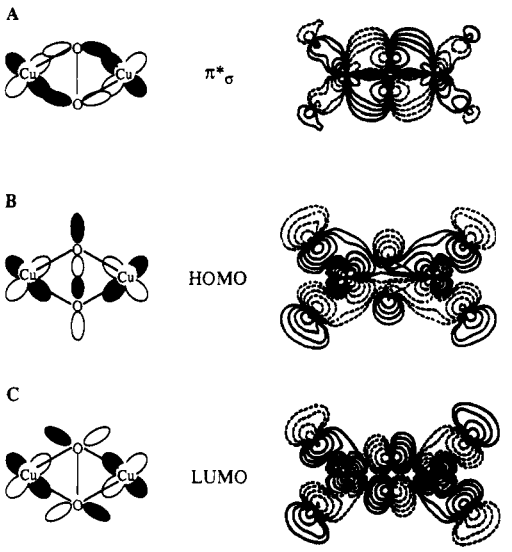

Figure 12. Schematic representations (left) and contour plots of coefficients of electron density (right) of the (A) π^*_σ, (B) HOMO, and (C) LUMO orbitals of the side-on model, from the broken-symmetry Xα calculations in ref 13.

of the side-on peroxide-bridged copper dimer. The experimental results from these studies can be compared to the electronic structure predicted by the broken-symmetry SCF-Xα-SW calculations by Ross and Solomon,[14] as well as to the experimentally derived electronic structure of the end-on bridged dimer.[9] The orbitals involved in copper–peroxide bonding in the side-on bridged structure are shown in Figure 12 by the contours of the electron densities from the Xα calculations. The σ-bonding interactions of the peroxide π^*_σ orbital are shown in Figure 12A, the π acceptor interaction of the peroxide σ^* orbital in the HOMO is demonstrated in Figure 12B, and the antibonding interaction of the π^*_σ orbital with the coppers in the LUMO is shown in Figure 12C.

The intensities of the peroxide-to-copper charge-transfer transitions probe the amount of $Cu(d_{x^2-y^2})$ character in the predominantly peroxide π^*_σ molecular orbital, allowing comparison of the charge donation from the peroxide to the coppers. The ratio of 1:1.9:3.7, or about 1:1:2 per copper, was derived for the relative amount of $Cu(d_{x^2-y^2})$ character in the predominantly peroxide π^*_σ molecular orbital in the series monomer → end-on dimer → side-on dimer. This ratio shows that the amount of peroxide donation to the copper is proportional to the number of coordination positions occupied by the peroxide: one in the monomer, two in the end-on dimer, and four in the side-on dimer. This trend was predicted by the Xα calculations,[14] which gave a ratio of peroxide character in the LUMO for the end-on:side-on dimers of 1:2 to 2:3. This experimentally derived ratio is important in two respects. First, it indicates that the number of peroxide–copper σ-bonding interactions may be determined on the basis of experimentally accessible parameters in the absorption spectrum, even if the precise structure is not known, such as for oxyhemocyanin [vide infra]. Second, it shows that the magnitude of the negative charge on the peroxide should follow the trend: side-on dimer < end-on dimer < monomer. This would be expected to result in a stronger O–O bond for the side-on bridged dimer, as electron density is donated from the π^*_σ orbital which is antibonding with respect to the O–O bond. However, this assumes that only σ donor bonding interactions are present for the peroxide, which is generally assumed to be the case.

The O–O force constants, which correlate to the O–O bond strength, were determined by normal coordinate analysis of the vibrational data from the peroxide–copper monomer,[8] the end-on peroxide-bridged copper dimer,[9] and the side-on peroxide-bridged copper dimer. The normal coordinate analysis shows that the O–O force constant for the side-on bridged dimer is 2.4 mdyn/Å, compared to O–O force constants of 2.9 mdyn/Å for the monomer and 3.1 mdyn/Å for the end-on dimer. As expected from their relative peroxide charges derived above, the end-on monomer has

a stronger O–O bond than the monomer. This is due to the donation of more antibonding electron density from the intra-peroxide bond in the dimer than in the monomer. This trend does not hold, however, in going to the side-on bridged dimer. Rather than an O–O bond which is stronger still, this complex has a significantly weaker O–O bond. This was predicted by the Xα calculations, which showed a unique interaction of the unoccupied peroxide σ^* orbital with the HOMO (Figure 12B) of the side-on bridged model only. Even a small amount of this kind of π back-bonding of electron density into the highly antibonding σ^* orbital of the peroxide significantly weakens the O–O bond, despite the lower total negative charge on the peroxide.

The usual correlation between force constant and bond length is not seen between the end-on and side-on bridged dimers. Although Badger's rule[31] predicts a longer bond in the side-on complex than in the end-on complex by about 0.07 Å on the basis of the O–O force constants, the X-ray crystal structures show O–O bond lengths of 1.412 Å for the side-on complex[13] and 1.432 Å for the end-on complex.[10] This is due to the fact that in complex molecules like these, especially with the closed ring geometry of the Cu_2O_2 unit of the side-on complex, the bonds have significant mechanical interactions so that the lowest energy bond length for one bond may not result in the lowest total energy configuration for the complex as a whole. Specifically, in the side-on model, for the O–O bond length to be longer as Badger's rule would predict, either the Cu–Cu distance must shorten or the Cu–O bonds must lengthen. The crystal structure[13] shows significant steric interaction between the R groups of the chelating ligand systems which prevents the coppers from moving closer together. Additionally, the Cu–O bonds of the side-on dimer are 0.06 Å longer than those of the end-on dimer in the crystal structures. Thus, the total energy of the side-on bridged structure appears to be minimized with a somewhat shorter O–O bond length than predicted by Badger's rule due to its dependence on the Cu–O bond lengths.

In addition to the ν(O–O) vibrations found in the resonance Raman spectra of $[Cu(HB(3,5\text{-}i\text{-}Pr_2pz)_3)]_2(O_2)$ at 749 cm^{-1} and $[Cu(HB(3,5\text{-}Ph_2pz)_3)]_2(O_2)$ at 763 cm^{-1}, three other vibrations of the Cu_2O_2 core of $[Cu(HB(3,5\text{-}Ph_2pz)_3)]_2(O_2)$ were found at 284, 331, and 572 cm^{-1} (based on an overtone at 1144 cm^{-1}). The 331 cm^{-1} vibration, identified in the infrared spectrum, is assigned for the D_{2h} point group as the B_{2u} mode in Figure 9. The 572 cm^{-1} fundamental of the 1144 cm^{-1} overtone identified in the resonance Raman spectrum is assigned as either the B_{1g} or B_{3u} mode, neither fundamental of which should have resonance intensity and both of which are expected to be in this energy region on the basis of normal coordinate analysis. The 763 and 284 cm^{-1} peaks (at 749 and 285 cm^{-1} in the R = *i*-Pr complex), which are both strong peaks in the resonance Raman spectra, are assigned as the two A_g modes. The higher frequency mode is mostly a change in O–O bond length, and the lower frequency mode is mostly a change in Cu–Cu distance. The difference in frequency is due largely to the difference in mass of the oxygen and copper atoms, as well as the lower force constant for the Cu–O bonds than for the O–O bond. For the end-on dimer and the monomer, in which the lower frequency totally symmetric mode is mostly a change in the Cu–O bond length, this mode is found at 488 and 561 cm^{-1}, respectively.[8,9] For peroxide bound side-on to a single transition metal ion, rather than bridging two metals as in this case, the symmetric ν(M–O) frequency is observed in the same range as those of the end-on copper–peroxide complexes.[32] For these side-on bound MO_2 complexes, this ν_s(M–O) mode would look like the B_{3u} mode in Figure 8, if one of the two coppers were missing, which has a similar frequency. Thus, the unexpectedly low frequency for the lower frequency A_g mode in the side-on bridged complex is due to the mechanical interactions unique to the side-on bridging structure which cause one of the totally symmetric modes to be mostly a "Cu–Cu stretch". The non-totally symmetric modes, which have mostly Cu–O character (B_{1g} and B_{3u} in Figure 8), are at frequencies expected for ν(Cu–O) modes, but they are not resonance enhanced and are therefore not observed in the resonance Raman spectrum.

The enhancement profiles of the totally symmetric vibrational modes provide information about the distortions which the molecule undergoes upon transition to its excited states. This in turn probes the changes in electronic structure between the ground and excited states. The resonance intensity is proportional to the square of the change in equilibrium distance of the nuclei and to the square of the absorption intensity of the resonant electronic transition.[25] We see from the enhancement profile of the ν(O–O) peak (in Figures 3–5) that the π^*_v transition causes a distortion mainly along the O–O bond due to a transfer in the antibonding electron density from the O–O bond to the Cu–O bond. The π^*_σ transition causes a smaller distortion along this mode, reflecting a similar change but to a lesser degree, while the much greater enhancement of the 285 cm^{-1} mode in Figures 10 and 11 indicates a large distortion along the Cu–O bonds due to transition from the strongly bonding (along Cu–O) π^*_σ orbital (Figure 12A) to the antibonding LUMO (Figure 12C).

B. Electronic Structure of Oxyhemocyanin and Oxytyrosinase and Its Relevance to Protein Function. The ground state of oxyhemocyanin is strongly antiferromagnetically coupled, with the singlet–triplet splitting $-2J > 600$ cm^{-1}.[33] Methemocyanin, which contains a fully oxidized active site $[Cu^{II}_2]$ but without a peroxide bond, is also strongly antiferromagnetically coupled.[34] The antiferromagnetism of the met site must be mediated by a super-exchange pathway other than a peroxide bridge, and an endogenous[35] bridging ligand, likely OH^-, must be present as part of the methemocyanin active site. Model complexes with no bridging ligand other than peroxide have been shown to be strongly antiferromagnetically coupled,[36] indicating that an additional bridge is not required for the strong coupling of the oxyhemocyanin site if peroxide bridges the site. This large singlet–triplet splitting in the peroxide-bridged copper dimers is related to the HOMO/LUMO splitting between the in-phase and out-of-phase combinations of the half-occupied copper orbitals.[14] This splitting is expected to be significantly greater for the side-on model than the end-on due to greater destabilization of the LUMO by the four σ bonds with peroxide compared to two in the end-on model and the stabilization of the HOMO in the side-on model by interaction with the peroxide σ^* orbital. However, the experimentally observed lower limits of $-2J > 600$ cm^{-1} for the end-on dimer by Karlin[36] and $-2J > 800$ cm^{-1} for the side-on dimer in this work show that either the end-on or side-on bridging geometries may be consistent with the strong antiferromagnetic coupling of oxyhemocyanin. A non-peroxide bridge is still required to explain the antiferromagnetism of methemocyanin.

Oxyhemocyanin produces unique optical spectra with intense absorption bands at 350 ($\epsilon \approx 20\,000$ M^{-1} cm^{-1}) and 580 nm ($\epsilon \approx 1000$ cm^{-1}), as well as a circular dichroism band at 480 nm with little corresponding absorption intensity. All of these features are absent in methemocyanin, and they have been assigned as peroxide-to-copper charge-transfer transitions, indicating that the peroxide must bridge the coppers.[1] Three bridging modes of peroxide with any transition metal ion were known at the time: a μ-1,1, a trans-μ-1,2, and a cis-μ-1,2 mode. On the basis of a transition dipole vector coupling analysis and the Cu–Cu distance derived from EXAFS, the μ-1,1 and trans-μ-1,2 models were ruled

(31) Hershbach, D. E.; Laurie, V. W. *J. Chem. Phys.* **1961**, *35*, 458–463.
(32) (a) Nakamura, A.; Yoshitaka, T.; Yamamoto, M.; Otsuka, S. *J. Am. Chem. Soc.* **1971**, *93*, 6052–6058. (b) Huber, H.; Klotzbücher, W.; Ozin, G. A.; Van der Voet, A. *Can. J. Chem.* **1973**, *51*, 2722–2736.

(33) (a) Solomon, E. I.; Dooley, D. M.; Wang, R.-H.; Gray, H. B.; Cerdonio, M.; Mogno, F.; Romani, G. L. *J. Am. Chem. Soc.* **1976**, *98*, 1029–1031. (b) Dooley, D. M.; Scott, R. A.; Ellinghaus, J.; Solomon, E. I.; Gray, H. B. *Proc. Natl. Acad. Sci. U.S.A.* **1978**, *75*, 3019–3022.
(34) (a) Wilcox, D. E.; Long, J. R.; Solomon, E. I. *J. Am. Chem. Soc.* **1984**, *106*, 2186–2194. (b) Wilcox, D. E.; Clark, P. A.; Solomon, E. I. Unpublished results.
(35) The term "endogenous" is used here to indicate a ligand which is intrinsic to the protein solution and is not displaced by addition of "exogenous" ligands.
(36) Karlin, K. D.; Tyeklär, Z.; Farooq, A.; Jacobson, R. R.; Sinn, E.; Lee, D. W.; Bradshaw, J. E.; Wilson, L. J. *Inorg. Chim. Acta* **1991**, *182*, 1–3.

out for the active site of oxyhemocyanin. In fact, Karlin has prepared model complexes with both the μ-1,1[37] and trans-μ-1,2[9] bridging models, and they are both spectroscopically very different from oxyhemocyanin. Thus, the cis-μ-1,2 peroxide bridge with an accompanying endogenous bridge was generally thought to be a model for the active site of oxyhemocyanin, consistent with the known spectral data.

In 1989, the X-ray crystal structure of the side-on peroxide-bridged copper dimer, $[Cu(HB(3,5\text{-}i\text{-}Pr_2pz)_3)]_2(O_2)$ was published.[13] This was the first known case of this μ-η^2:η^2 structure for a transition metal complex.[38] The Cu–Cu distance in this complex is nearly the same as for oxyhemocyanin, and the transition dipole vector coupling analysis presented in section D of the Results and Analysis section indicates that this structure is also consistent with the spectral features of oxyhemocyanin. The electric dipole-allowed components of the π^*_σ and π^*_v transitions at 350 and 570 nm in the absorption spectrum of oxyhemocyanin correspond to those at 350 ($^1B_{3u}$ in Figure 9) and 538 nm ($^1B_{1u}$) in the side-on complex. In addition, the electric dipole-forbidden component of the π^*_v transition ($^1B_{2g}$) is magnetic dipole allowed in the idealized D_{2h} geometry of the site. The 480-nm CD feature in oxyhemocyanin corresponds to this transition, gaining CD intensity by the small distortion away from any ideal symmetry in the protein site. Finally, this complex may be converted into bis-μ-OH and μ-N_3^-, μ-OH complexes,[17] consistent with the OH^- bridge required as a superexchange pathway in methemocyanin. This side-on bridging structure has thus become an attractive model for the active site of oxyhemocyanin.

These two models, the side-on and cis end-on, cannot be directly compared experimentally since there is no structurally characterized copper model with the cis-μ-1,2 bridging mode. However, our Xα calculations[14] showed that an end-on cis-μ-1,2 model should have an electronic structure similar to that of the structurally characterized end-on trans-μ-1,2 complex, but an electronic structure significantly different from that of the side-on μ-η^2:η^2 complex. These calculations do not take into account the excited-state splittings mediated by dimer interactions, however, so that the observed absorption spectrum for the trans complex cannot be directly correlated to that which would be found for a cis model. The low O–O force constant is a better indicator that oxyhemocyanin has the side-on structure since a normal coordinate analysis showed that mechanical interactions would slightly raise the frequency in the cis relative to the trans model if the force constant is the same. However, it could be argued that a hydroxide bridge in the cis model would donate electron density to the peroxide through the coppers, thus weakening the O–O bond. It has also been suggested that a hydrophobic active site environment in the protein could lower the frequency.[11]

One parameter which has been investigated above that must be different for the end-on cis and side-on models is the relative amount of peroxide σ donation to the coppers. It was shown by comparison of the end-on and side-on complexes to the peroxide–copper monomer that the integrated intensity of the peroxide-to-copper charge-transfer transitions is directly related to the number of peroxide–copper σ donor interactions, which is two for the cis end-on model and four for the side-on model. The ratio of peroxide donation to the coppers in the series monomer:end-on dimer:side-on dimer is 1:1.9:3.7. The relative values derived for oxyhemocyanin in Table II are 3.7 if a side-on geometry is assumed and 3.6 if a cis end-on geometry is assumed. A value much greater than 2 relative to the monomer is not reasonable for an end-on binding mode, in which the peroxide occupies only one coordination position on each copper. The value of 3.7 for a side-on model of oxyhemocyanin, however, quantitatively corresponds with that derived for the structurally characterized side-on peroxide-bridged copper dimer. It appears, therefore, that the active site of oxyhemocyanin has peroxide occupying four copper coordination positions and thus contains a side-on peroxide bridge between the two Cu(II)'s.

The electronic structure of this side-on peroxide bridging model for the active site of oxyhemocyanin allows us to understand the unique spectral features of oxyhemocyanin. The unusually high intensity of the absorption band at 350 nm is due to the four peroxide–copper σ donor interactions. In addition, the four interactions should stabilize the π^*_σ orbital in the side-on geometry more than the two σ donor interactions in the end-on geometry. The observed energies of the transitions are not directly related to this difference, since the transitions are split by dimer interactions which will be different for each geometry. However, the splittings should be greater for the side-on geometry, so that the higher observed energy for the 350-nm transition in oxyhemocyanin and the side-on model complex compared to the end-on model complex does reflect the greater stabilization of the π^*_σ orbital in the side-on geometry. The unusually low O–O stretching frequency in oxyhemocyanin[11,12] is also explained by the studies on the side-on bridged model complex. Although the greater σ donation from the side-on bridge relative to the end-on bridge removes π-antibonding character from the O–O bond (Figure 12A), back-donation into the unoccupied peroxide σ^* orbital puts a limited amount of electron density into a highly antibonding molecular orbital, which significantly weakens the bond (Figure 12B). The unusual electronic structure of the side-on bridge thus allows for the seemingly contradictory less negative peroxide with a weaker O–O bond. Finally, the lack of a symmetric Cu–O stretching peak between 400 and 600 cm^{-1} in the resonance Raman spectrum of oxyhemocyanin[10,11] is explained by the unique mechanical interactions in the closed ring of the side-on bridged geometry. The motion which would give the symmetric Cu–O stretch in a side-on bound peroxide–copper monomer becomes an antisymmetric B_{3u} vibration when the second copper is added, so that this vibration can have no *A*-term resonance enhancement in the centrosymmetric site. There is a strong feature in the resonance Raman spectrum of oxyhemocyanin[11,12] at about 267 cm^{-1} for the molluscs and between 280 and 290 cm^{-1} for the arthropods which has enhancement behavior similar to that of the 285 cm^{-1} feature in the resonance Raman spectrum of the side-on model complex. This feature has been assigned as an imidazole nitrogen–copper stretch[11,12] due to its lack of an oxygen isotope shift and a small but measurable shift in frequency when the protein is placed in D_2O. However, the normal coordinate analysis of the vibrational data for the side-on model complex shows that there should not be a measurable oxygen isotope shift for the lower frequency A_g mode ("ν(Cu–Cu)" in Figure 8). In addition, resonance Raman studies on azide methemocyanin showed[39] that the bound azide interacts with the protein pocket. Such an interaction with the peroxide could be sufficiently perturbed by changing the solvent from H_2O to D_2O to produce the small observed deuterium isotope shift for the Raman peak in oxyhemocyanin.

The most compelling reason for defining protein active site geometry and electronic structure is to understand the relationship between the structure and function of the protein. These studies of the electronic structure of the side-on bridged model and comparison of its properties to those of the end-on complexes provide insight into the reactivities of oxyhemocyanin and oxytyrosinase. An important feature of oxyhemocyanin as an oxygen transport protein is its ability to bind oxygen as peroxide sufficiently strongly to prevent loss of peroxide from the copper site, resulting in the inactive met protein. Figure 13 shows energy level diagrams of the valence orbitals of the end-on (A) and side-on (B) peroxide-bridged models. The greater σ donation in the

(37) (a) Ghosh, P.; Tyeklár, Z.; Karlin, K. D.; Jacobson, R. R.; Zubieta, J. *J. Am. Chem. Soc.* **1987**, *109*, 6889–6891. (b) Karlin, K. D.; Cruse, R. W.; Gultneh, Y. *J. Chem. Soc., Chem. Commun.* **1987**, 599–600.

(38) (a) Structurally defined side-on μ-η^2:η^2 peroxide-bridged actinide[38b] and lanthanide[38c] complexes had been previously reported and, more recently, a dibridged vanadium dimer with bent μ-η^2:η^2 peroxide and fluoride bridges has been structurally characterized.[38d] (b) Haegele, R.; Boeyens, J. C. A. *J. Chem. Soc., Dalton Trans.* **1977**, 648–650. (c) Bradley, D. C.; Ghotra, J. S.; Hart, F. A.; Hursthouse, M. B.; Raithby, P. R. *J. Chem. Soc., Dalton Trans.* **1977**, 1166–1172. (d) Lapshin, A. E.; Smolin, Y. I.; Shepelev, Y. F.; Schwendt, P.; Gyepesova, D. *Acta Crystallogr.* **1990**, *C46*, 1755–1759.

(39) Pate, J. E.; Thamann, T. J.; Solomon, E. I. *Spectrochim. Acta* **1986**, *42A*, 313–318.

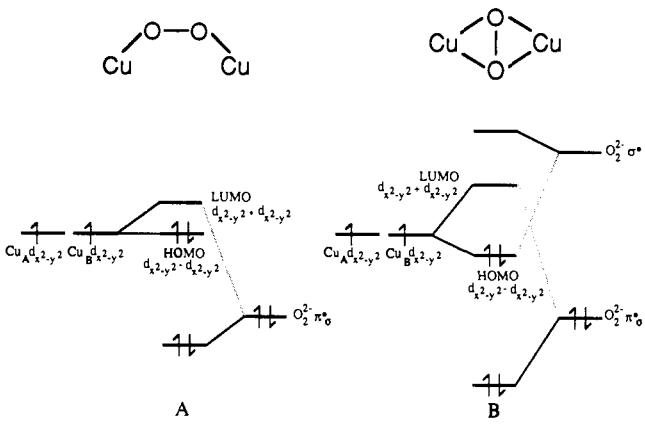

Figure 13. Energy level diagrams of the orbitals involved in copper–peroxide bonding in (A) end-on bridged and (B) side-on bridged models.

side-on case strengthens peroxide bonding compared to the end-on case, as demonstrated by the greater stabilization of the π^*_σ levels in Figure 13. The HOMO is additionally stabilized in the side-on model compared to the end-on model due to the π acceptor interaction of the peroxide σ^* orbital. Together these produce the greater stability of the side-on bridged Cu_2O_2 unit compared to the end-on bridged Cu_2O_2 unit with respect to decomposition to a Cu(II) product with loss of peroxide. This explains the significantly greater thermal stability of the side-on bridged dimer complex (stable below about −10 °C) than of the end-on bridged monomer or dimer complexes (unstable above about −70 °C).

The electronic structure of the side-on peroxide bridging model also provides an electronic mechanism for the activity of oxytyrosinase, in which peroxide bridges the binuclear copper site in the same manner as in oxyhemocyanin.[3] Tyrosinase activates O_2 for reaction with phenols, oxygenating them to *o*-diphenols.[40] The key presence of some peroxide σ^* character in the HOMO (Figure 12B) greatly weakens the O–O bond, activating it for cleavage. In addition, the greater σ donation from peroxide in the side-on geometry, indicated by the stabilization of the π^*_σ orbital in Figure 13, results in a less negative peroxide, which contributes to attack by the electron-rich substrate. We have demonstrated that for tyrosinase the monophenol substrate binds directly to the copper at the active site.[3,41] Charge donation by this bound substrate into the LUMO (Figure 12C), which is strongly antibonding in both the O–O and Cu–O bonds, further activates these bonds toward cleavage and oxygen transfer to the substrate.

In summary, these studies have experimentally defined the unique electronic structure of the side-on peroxide-bridged copper dimer. An analysis of the intensity of the peroxide-to-copper charge-transfer transitions shows that the peroxide undergoes four σ donor interactions with the two coppers, so that the peroxide occupies two coordination positions on each copper. These four σ donor interactions produce a less negative peroxide than in the end-on bridged dimer. However, the normal coordinate analysis of the vibrational data shows that the O–O bond is significantly weaker than in the end-on bound copper–peroxide complexes. This provides direct experimental evidence for the interaction of the unoccupied peroxide σ^* orbital with the HOMO in which a small amount of electron density is donated by the copper into a highly antibonding π acceptor orbital of the peroxide. A quantitative comparison of the absorption intensity of the peroxide-to-copper charge-transfer transitions in oxyhemocyanin to the monomer → end-on dimer → side-on dimer series shows that the active site of oxyhemocyanin has four peroxide–copper bonds and thus has the side-on μ-η^2:η^2 peroxide bridging structure. The electronic structure of this side-on bridging model for the active site of oxyhemocyanin provides understanding of its unique spectral features, including the high intensity of the 350-nm absorption band, the unusually low O–O stretching frequency, and the lack of a ν_s(Cu–O) Raman feature in the "normal" range of 400–600 cm^{-1} but the presence of a strongly enhanced resonance Raman feature below 300 cm^{-1}.

Acknowledgment. The authors thank Dr. Felix Tuczek for helpful discussions regarding charge-transfer excited-state splittings. N.K. and K.F. thank Professor Yoshihiko Moro-oka of the Tokyo Institute of Technology for continuous encouragement in completing the present work. This research is supported by National Institutes of Health Grant DK 31450 (E.I.S.) and the Japanese Ministry of Education, Science, and Culture Grant-in-Aid for Scientific Research 03241106 (N.K.).

(40) Jolley, R. L., Jr.; Evans, L. H.; Makino, N.; Mason, H. S. *J. Biol. Chem.* **1974**, *249*, 335–345.

(41) Winkler, M.; Lerch, K.; Solomon, E. I. *J. Am. Chem. Soc.* **1981**, *103*, 7001–7003.